Journal of Cluster Science (2021) 32:1701–1709
https://doi.org/10.1007/s10876-020-01939-9

ORIGINAL PAPER

Visible Light Photocatalyst Anatase Phased TiO_2 Nanoparticles for Enhanced Antibacterial Performance

G. Nagaraj[1] · S. Tamilarasu[2]

Received: 28 June 2020 / Accepted: 3 November 2020 / Published online: 12 November 2020

Abstract

This study reports the development of anatase TiO_2 synthesized by facile photon-induced method (PIM) at various reaction times of 6 days, 8 days, 10-day samples. The 10 days TiO_2 sample shows stable anatase phase, whereas 100% rutile phase at the same temperature was observed for standard TiO_2. Mainly, the PIM was used to tuning the properties of visible light absorbance TiO_2 photocatalyst used for improving antibacterial performance. The antibacterial activity of TiO_2 against *Staphylococcus aureus* and *Escherichia coli* was determined by the agar disc diffusion method. Anatase TiO_2 nanoparticles demonstrated excellent antibacterial activity against extracellular *S. aureus* with 80% and *E. coli* with 82% killing efficacy at concentrations as low as 100 µg/mL, which is 100% faster than the standard and other pure TiO_2 reported earlier. The obtained undoped anatase Titania with enhanced chemical reactivity has great potential for antibacterial properties. Moreover, the smaller crystallite size (25 nm) and narrowing bandgap (2.96 eV) TiO_2 nanoparticles were more effective in killing bacteria compared with standard TiO_2. Therefore, this work indicated that anatase phased TiO_2 under visible light absorbance has good potential with excellent clinical applications.

Keywords Pure titania · PIM · Antibacterial · Oxygen-rich · High phase stability

Introduction

The semiconductor-based photocatalysis has received great attention in recent times. The reason is that it is inexpensive, has good photostability and is environmental friendly for the elimination of organic contaminants in the waste-water by using renewable solar energy [1–4]. Moreover, photocatalysis is also known as green technology as it eliminates organic contaminants into nontoxic molecules of CO_2, H_2O and mineral acids without producing any secondary pollution [5–7]. The titanium-di-oxide (TiO_2) has great potential in many research fields such as solar cells, batteries, self-cleaning, antibacterial, and cancer therapy so far [8–13]. The TiO_2 is used as a promising photocatalyst material to deal with energy and environmental application owing to its better behavior of non-toxicity, high chemical inertness, and good photo-stability [14, 15]. The influence of structure and surface properties of TiO_2, such as phase type [16], particle size [17], surface area [18], crystallinity [19] and oxygen vacancy concentration [20] on its photocatalytic activities have been extensively investigated so far. The large application of TiO_2 photocatalyst is strongly hindered in visible-light due to its low absorption in the solar light spectrum and rapid recombination of photo-excited electron and hole pairs via the band-gap energy of 3.2 eV. Hence, the focused synthesis of highly visible-light active TiO_2 photocatalyst is the most important task for practical application [21–27]

In this regard, researchers are focusing to prepare high visible-active TiO_2 nanoparticles through numerous methods. A high-temperature stable oxygen-rich TiO_2 was prepared from thermal decomposition of the peroxo-titania complex through a precursor modification with H_2O_2 by Etacheri et al. [28] and Tan et al. [29]. Meanwhile, Jadhar et al. [30] also synthesized oxygen-rich TiO_2 through precursor modification with the help of H_2O_2. L. LV et al. [31] prepared highly stable TiO_2 with pure anatase phase from the tri-fluoro acetic acid (TFA) solution. In addition,

✉ G. Nagaraj
thomsun1977@gmail.com

[1] Department of Physics, Periyar University P.G Extension Center, Dharmapuri, Tamil Nadu, India

[2] Department of Physics, Jayam Arts and Science College, Periyar University, Salem, Tamil Nadu, India

K. LV et al. [32] reported the thermally stable anatase phase TiO_2 from $TiOF_2$ precursor with increased photocatalytic ability under visible-light illumination. Apart from that, many researchers have found the best percentage of the mixed phases in the TiO_2 [33–35]. According to these reports, it can be found that pure anatase TiO_2 exhibited an improved photocatalytic ability toward the removal of organic pollutants compared with pure rutile and mixed phased TiO_2, which is attributed to the lower recombination rates in pure anatase TiO_2.[36, 37]. Also, the pure anatase-phased TiO_2 nanoparticles have low thermal stability up to a maximum temperature of 650 °C. However, researchers have reported that the anatase phase stability can be improved by increasing the oxygen content of the sample and achieving pure anatase-phased TiO_2 nanoparticles up to 800 °C with better photocatalytic activity [38, 39]

In this work, we have synthesized a highly stable anatase-phased TiO_2 nanoparticles even up to 900 °C by using a simple and low-cost new synthesis method of photon-induced method [26, 27, 38, 40, 49, 50]. The anatase phased pure TiO_2 nanoparticles showed strong solar-light absorption ability with low bandgap energy of 2.96 eV. However, the pure anatase TiO_2 nanoparticles exhibited enhanced photodegradation of methylene blue (MB) using a solar-light illumination within 15 min reported earlier [40]. Here, a comparison of the properties of pure Titania prepared by other synthesis methods and pure Titania prepared by new Photon induced method is presented in Table 1. Therefore, the obtained pure anatase TiO_2 nanoparticles with high phase stability from PIM will be potential photocatalytic materials for clinical applications.

Materials and Methods

Materials

Titanium tetra isopropoxide of AR grade were purchased from Sigma Aldrich and Double Distilled water.

Preparation of Anatase TiO_2

A simple and low-cost-photon induced method (PIM) was employed to synthesize pure anatase TiO_2 nanoparticles. Briefly, 600 mL of double-distilled water and the required quantity of titanium tetra-isopropoxide (TTIP, 2 mL) were mixed together and continuously stirred for 6 days, 8 days and 10 days under the illumination of halogen light. Then, this solution was allowed to dry under a halogen lamp to collect a white powder. Finally, the collected PIM-prepared powder was calcined at 900 °C for 1 h and standard P25-TiO_2 was calcined at 900 °C for 1 h.

Antibacterial Studies

The antibacterial activity of anatase TiO_2 was examined by the Agar diffusion well method. Four serial dilutions yielded concentrations of 100, 75, 50, and 25 mg were other alone into 4 Petri disks for extracts. Gram-negative *Escherichia coli* (*E. coli*) and Gram-positive *Staphylococcus aureus* (*S. aureus*) were incubated at 37 °C for 24 h and was used to analyze the antibacterial perform of nanomaterials. The antibacterial perform of nanomaterials was under the dark and solar-light from 12:00 PM to 1:00 PM. Reference commercial disks used Chloramphenicol 30 mg. After that, the incubation confluent bacterial growth was detected and bacterial growth was measured in mm.

Results and Discussion

XRD Analyssis

Figure 1 illustrates the XRD patterns of standard pure TiO_2 and PIM samples have been prepared for 6 days, 8 days and 10 days, respectively, which were calcined at 900 °C. Figure 1a, b corresponds to standard pure TiO_2 and PIM in 6-day samples, the peaks corresponding to the rutile phase alone are observed (JCPDS # 21–1276), PIM- 8 days

Table 1 comparison of the properties of pure Titania

TiO_2 prepared by other methods (Standard pure TiO_2)	TiO_2 prepared by new photon induced method (PIM)
Pure anatase phase stable below 600 °C	Pure anatase phase stable above 900 °C
Anatase phase bandgap energy is 3.2 eV(600 °C)	Anatase phase bandgap energy is 2.96 eV
Visible-light photocatalytic activity (0%)	Visible-light photocatalytic activity (100%)
Particles size above 25 nm (P25) (600 °C)	Particles size below 40–50 nm
Crystalline size above 20 nm (600 °C)	Crystalline size 16 nm
Oxygen vacancy	Oxygen rich
Antibacterial activity 0% (900 °C)	Antibacterial activity 80% (900 °C)

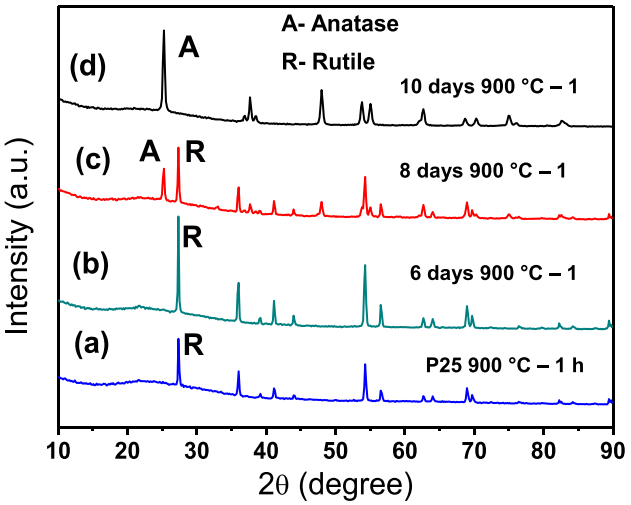

Fig. 1 XRD patterns of calcined at 900 °C **a** Standard Pure-TiO_2 (rutile phase), **b** PIM- 6 days prepared TiO_2 (rutile phase), **c** PIM- 8 days prepared TiO_2 (mixed phase) and **d** PIM- 10 days prepared TiO_2 (anatase phase)

sample mixed phase of anatase and rutile as shown in Fig. 1c, while PIM sample obtained in 10 days exhibit the similar characteristic diffraction peaks. It is shown that the pure anatase phased TiO_2 nanoparticles do not change the rutile phase. However, it can be noticed that the peak intensities of the anatase phase are dominant even at 900 °C. XRD peaks appeared for the calcination temperature of 900 °C at $2\theta = 25.27°$, 37.67°, 47.96°, 53.8°, 55.06°, 62.61°, 68.95°, 74.88° and 82.54° are ascribed to the (101), (004), (200), (105), (211), (204), (116), (215) and (224) hkl plane of anatase, correspondingly (JCPDS: 21–1272) as shown in Fig. 1d [28–30]. It may be noted that only anatase-phased TiO_2 has been found in a 10-day sample. This may be due to the increased oxygen content in the sample when increased with reaction time, which has increased the anatase phase stability. The average crystallite size of PIM is prepared for 6 days, 8 days, 10 days and standard pure are shown in Table 4.

Therefore, the pure anatase phase has retained even at high stability up to 900°C for 10 days whereas, the standard pure TiO_2, 6 days and 8 days samples exist at 100% rutile and mixed-phase calcined at 900 °C respectively. Clearly, the delayed effect on the synthesis method (photon effect) plays a major role in the process of phase transition. It is evident that the standard pure TiO_2 sample can lose its phase stability when calcined at 900 °C, which is confirmed through the emergence of peaks representing the rutile phase reported by Yoko et al. [41]

The lattice constant and d-spacing were calculated from the XRD data. The Bragg's law is used to calculate the lattice constant of the crystalline nanopowder. The lattice spacing of (0 0 2) and (0 0 4) oriented tetragonal crystals. The calculation of d-spacing used Bragg's law.

$$d = n\lambda/2\sin\theta \quad (1)$$

λ = 1.5406 Å, θ = Peak position, n = 1(order of diffraction) and d = interplaner spacing or d-spacing. Unit cell lattice constant (a = b ≠ c). The equation of interplaner spacing for a tetragonal unit cell is given by

$$1/d^2 = \left(h^2 + k^2\right)/a^2 + l^2/c^2 \quad (2)$$

where h, k and l is the miller indices, d is interplaner spacing a and c is the lattice constant of unit cell. The calculated lattice constant and d-spacing values given the Table 2 [42–44].

FT-IR Analysis

The FT-IR spectra of the standard pure TiO_2 nanoparticles from PIM prepared for 6 days, 8 days, 10 days are shown in Fig. 2a, b, c and d respectively. All the samples were attributed to Ti–O–Ti stretching. Vibrations were identified

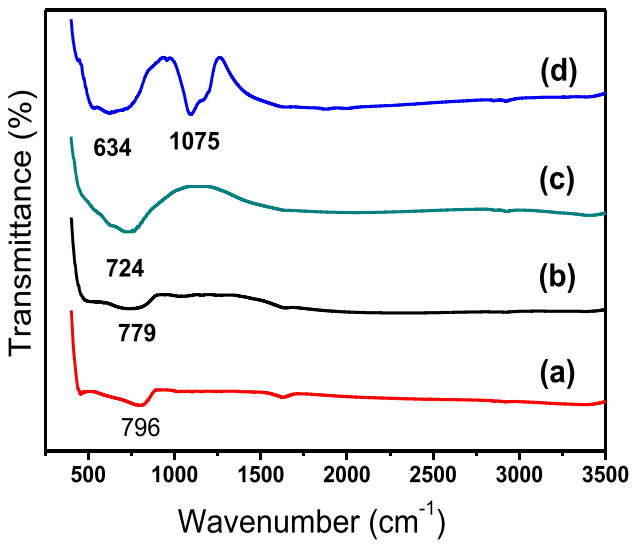

Fig. 2 FT-IR spectra of calcined at 900 °C **a** Standard Pure-TiO_2, **b** PIM- 6 days prepared TiO_2, **c** PIM- 8 days prepared TiO_2 and **d** PIM- 10 days prepared TiO_2

Table 2 PIM- 10 days anatase TiO_2 Lattice constant

h k l	d-Spacing (Å)	Lattice constant	Standard values	Our calculated values
2 0 0	3.7892	a = b	3.7848	3.7892
0 0 4	2.3852	c	9.5124	9.5421

Table 3 FTIR peaks with points value

Wavenumber (cm^{-1})				Vibrational assignments
(a) Standard	(b) 6 days	(c) 8 days	(d) 10 days	
796	779	724	634	Ti–O–Ti stretching
–	–	–	1075	C–O alkoxy stretching

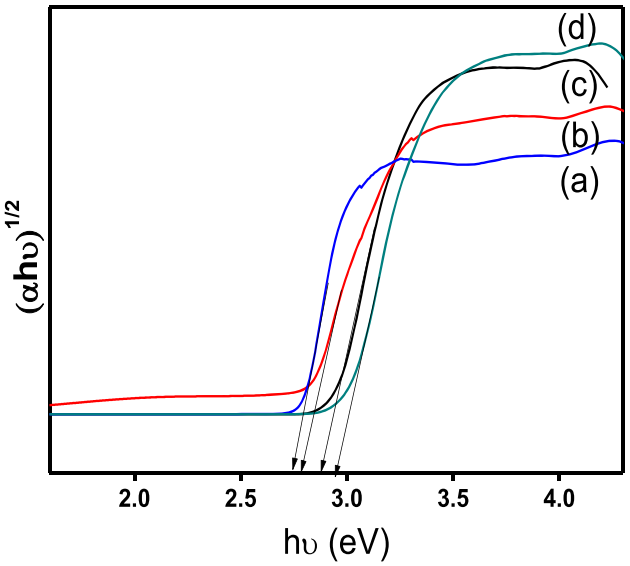

Fig. 3 UV-DR spectra of calcined at 900 °C **a** Standard Pure-TiO_2, **b** PIM- 6 days prepared TiO_2, **c** PIM- 8 days prepared TiO_2 and **d** PIM- 10 days prepared TiO_2

at 540–790 cm^{-1} [28, 29, 45, 46]. This peak confirms the synthesis of oxygen-rich TiO_2 nanoparticles. Also, the peak corresponding to the C–O bond is observed around 1075 cm^{-1} indicating C–O alkoxy stretching. The vibration was observed for the oxygen-rich TiO_2 sample shown in Fig. 2d. However, the C–O peak does not appear in the standard pure TiO_2 calcined at 900 °C [28, 38]. The FTIR peaks with point value given the Table 3. This discussion confirms that no chemical reduction occurred as the binary composites prepared. As a result, confirming the successful preparation of PIM pure Titania.

Optical Analysis

The optical properties of samples were assessed by the UV–Vis DRS test. The absorption properties of pure TiO_2 have been investigated by DRS. Figure 3a, b, c, and d shows the optical band gap determination for PIM prepared pure TiO_2 for 6 days, 8 days 10 days and standard pure TiO_2 samples calcined at 900 °C using the DRS reflection data modified Tauc relation given below [42–44, 47, 48]

$$\alpha h\upsilon = A(h\upsilon - Eg)^n \quad (3)$$

where α is the absorption coefficient, a constant and n the exponent that depends on the quantum selection rules for the particular material. A straight line is obtained when $\alpha h\upsilon^{1/2}$ is plotted against photon energy (hυ). The calculated indirect band gap of all samples is shown in Table 4. It has been reported that pure anatase phased TiO_2 is a wide bandgap semiconductor, and it can only absorb UV light. The reported bandgap of standard pure TiO_2 with anatase phase is 3.2 eV [2, 15], whereas the PIM prepared 10 days TiO_2 sample calcined at 900 °C exhibited the strong visible-light absorption ability by small bandgap energy of 2.96 eV shown in Fig. 3d [28, 44]. The bandgap also confirms the oxygen excess nature of the samples [28]. The results are similar to those observed by Gao et al. [46]. Reports on the upshift of valence band due to surface disorderliness are available [30]. This narrowing of the bandgap is expected to provoke the visible light-absorbing capacity of pure TiO_2.

Morphology Analysis

The surface morphology of the PIM- TiO_2 and standard pure TiO_2 samples with calcined at 900 °C was analyzed using HRSEM and HRTEM. Figure 4 shows typical HRSEM images of PIM-prepared TiO_2 for 6 days, 8 days, 10 days, and standard pure TiO_2. A detailed HRSEM investigation of the nanoparticle surface morphology states that the agglomerates for standard pure and PIM- 6 days sample shown in Fig. 4a and b, PIM—8 days and 10 days sample are uneven rods and roughly spherical in shape

Table 4 All characterization results

Sample calcined at 900 °C	Phase	Crystalline size	Bandgap	Particle size
P25-TiO_2	Rutile:100%	110 nm	2.74 eV	130–160 nm
PIM- TiO_2 for 6 days	Rutile:100%	82 nm	2.80 eV	95–110 nm
PIM- TiO_2 for 8 days	Mixed phase	42 nm	2.89 eV	50–70 nm
PIM- TiO_2 for 10 days	Anatase:100%	25 nm	2.96 eV	40–50 nm

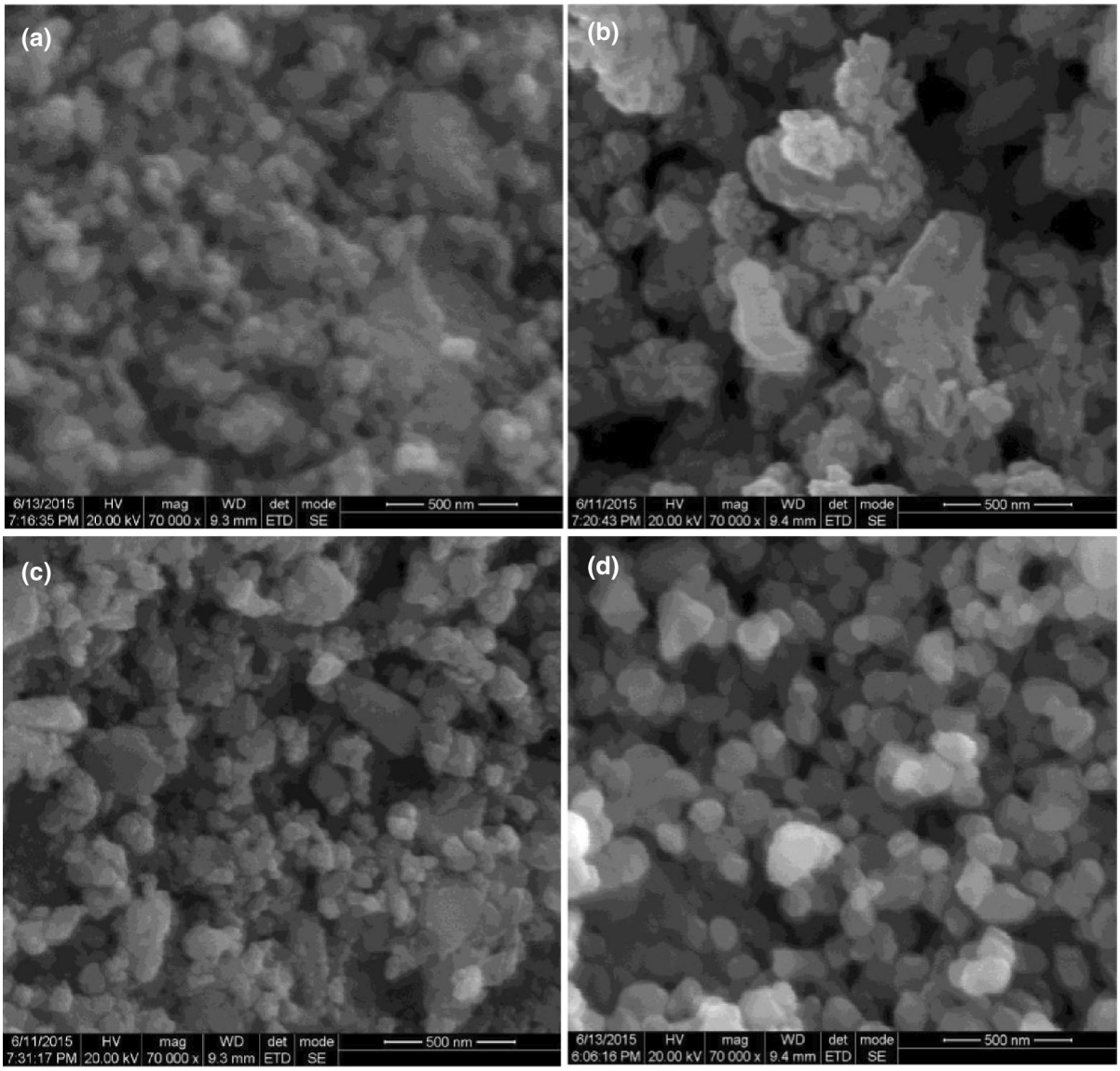

Fig. 4 HR-SEM image of calcined at 900 °C **a** Standard Pure-TiO_2, **b** PIM- 6 days prepared TiO_2, **c** PIM- 8 days prepared TiO_2 and **d** PIM- 10 days prepared TiO_2 particles

shown in Fig. 4c and d. High-Resolution Transmission Electron Microscopic (HRTEM) image corresponding to the TiO_2 samples calcined at 900 °C. Figure 5a standard pure TiO_2 sample rod like-structures, Fig. 5b 6 days sample show agglomerates, Fig. 5c 8-day sample rods like structures and 10 days sample particle like structures as shown in Fig. 5d. The diameters of the anatase TiO_2 were less than 40–50 nm. The high magnification HRTEM of 10 days-TiO_2 in Fig. 5e shows the appearance of the mesoporous structure on the surface of TiO_2 particles. Figure 5f the EDAX spectrum of pure anatase phased TiO_2. It is confirmed that only Ti and O are present in the samples. The standard pure TiO_2, PIM- 6 days, PIM- 8 days and PIM- 10 days TiO_2 samples calcined at 900 °C, the particle size is presented in Table 4.

Raman and Photoluminescence

Figure 6a shows the Raman spectrum of PIM- 10 day's anatase Titania calcined at 900 °C. The Raman peaks detected at 143 and 638 cm^{-1} are related to the E_g modes of anatase phase and also peak detected at 390 cm^{-1} maybe corresponds to the $B1_g$ mode. Likewise, the peak appeared at 515 cm^{-1} is a doublet of $A1_g$ and $B1_g$ modes for the anatase phase. Thus, it is clear that the sample exists pure anatase phase-only even when calcined at 900 °C.

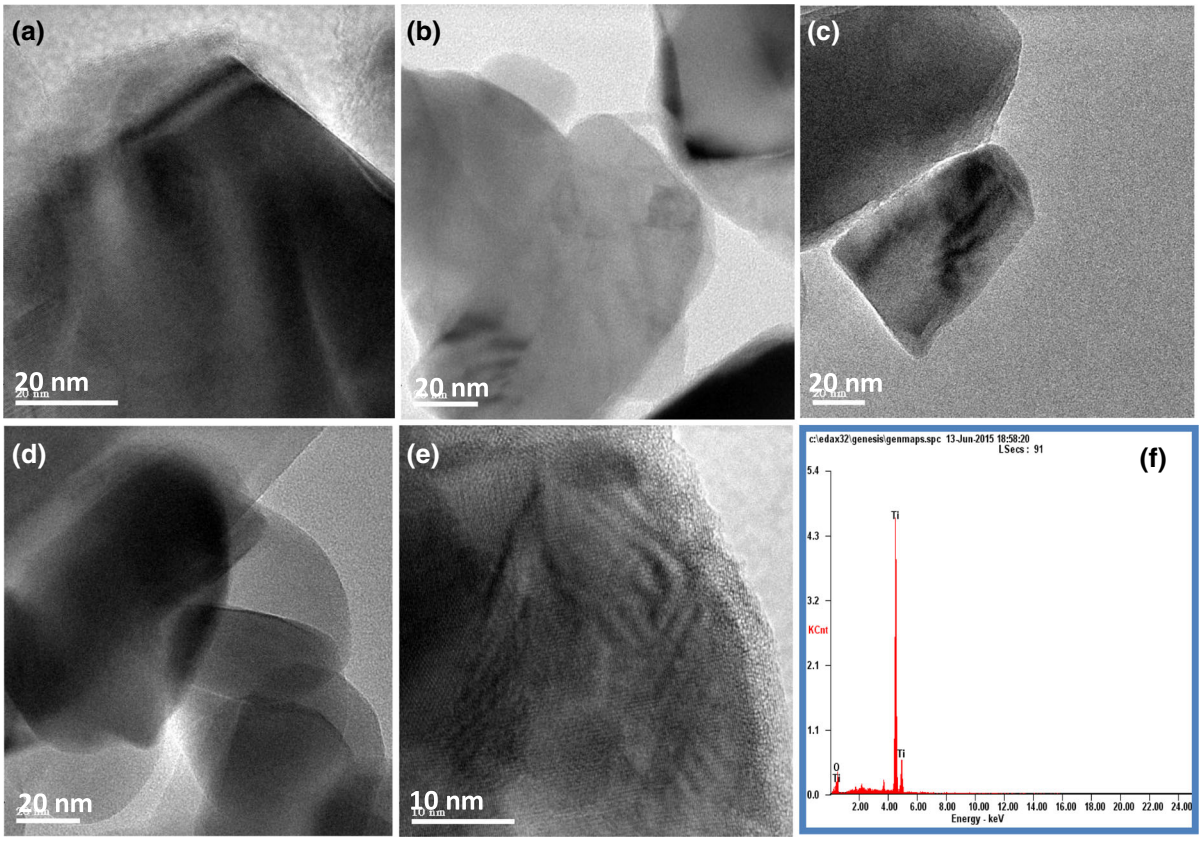

Fig. 5 HR-TEM images of calcined at 900 °C, **a** Standard Pure-TiO_2, **b** PIM- 6 days prepared TiO_2, **c** PIM- 8 days prepared TiO_2, **d** EDAX spectrum of anatase phased TiO_2 **e** PIM-10 days prepared TiO_2 and the zoom of Fig. **e** and **h** mesoporous structure

Figure 6b shows the PL spectrum of PIM- 10 days anatase TiO_2 nanoparticles calcined at 900 °C. As seen in Fig. 6b, the four prominent emission peaks are observed at 341, 564, 634 and 678 nm, which are attributed to the 5d-4f emission band of the TiO_2. The intense peaks at 564, 634, 678 nm are related to the $5D_0$-$7F_0$ transition. The strong emission peaks observed at 634 and 678 nm are due to the electrical dipole transition ($5D_0$-$7F_2$) of TiO_2 which gives the red color to the luminescence signals (visible region).

Antibacterial Analysis

The PIM prepared 10 days anatase TiO_2 nanoparticles are reported that it can range the spectral response to the visible region [27, 49, 50]. When the absorption range of TiO_2 is induced to the visible light region, the photocatalytic reaction occurs under the irradiation of solar light. These reactive oxygen species are toxic to the bacteria [51]. Antimicrobial activity of TiO_2 nanoparticles were investigated by well diffusion method against two bacterial strains, *E. coli*, and *S. aureus*. The results of zone inhibition method have been described from Fig. 7, it is seen that TiO_2 NPs show good inhibition zone around the films. The 10 days prepared PIM- TiO_2 nanoparticles as an antimicrobial agent were assessed against *Escherichia coli* (*E. coli*) and *Staphylococcus aureus* (*S. aureus*). We observed that the size of inhibition zones significantly increased when preserved with TiO_2 compared with zones of inhibition in case of control as shown in Table 5. The growth inhibition pattern of *Escherichia coli* (*E. coli*) and *Staphylococcus aureus* (*S. aureus*) with increasing concentrations of PIM- 10 days TiO_2 as shown in Fig. 7a and b. The maximum concentration of TiO_2 (100 mg) inhibits 80% and 82% of TiO_2 quantum dots by *S. aureus* and *E. coli*, respectively [52, 53]. Enhanced antibacterial activity by PIM-TiO_2 than standard pure TiO_2 (0%) was

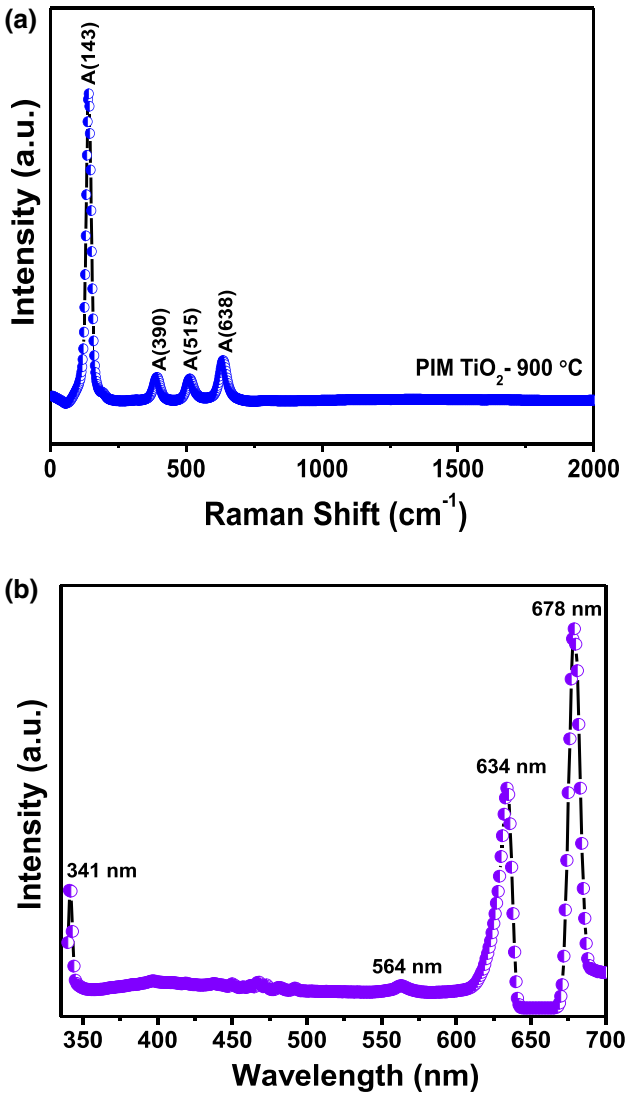

Fig. 6 **a** Raman, and 6 **b** Photoluminescence spectrum of anatase phased TiO_2 by PIM prepared 10 days with calcined at 900 °C

reported earlier [54, 55]. This results in a promising antimicrobial agent for inhibiting bacterial infections by Photon Induced Method prepared oxygen-rich anatase TiO_2.

Conclusions

Herein, the enhanced temperature stable with solar-light photocatalyst anatase TiO_2 nanoparticles was successfully obtained from a simple and low-cost PIM. A series of TiO_2 nanoparticles were synthesized through different reaction times in 6 days, 8 days and 10 days, respectively, at a calcined temperature of 900 °C. The phase transformation delay of anatase to rutile (PIM-TiO_2 for 10 days) is of great significance to the study of Titania. The optical properties of PIM-TiO_2 is greatly influenced by its crystallinity, surface areas, grain size, and surface hydroxyl content than standard TiO_2 earlier reports. This PIM-prepared TiO_2 for solar cells, cancer cells killed, antibacterial and photocatalysis applications under visible light. Standard TiO_2 and other TiO_2 samples only UV light photocatalytic activity. Most doping or H_2O_2 modified Titania ultimately increase the thermal stability of the anatase phase and visible light photocatalyst reported earlier. However, in our case, the absence of dopant or H_2O_2 Titania enhanced thermal stability with solar-light activity via a facile synthesis method (PIM) here reported for the first time. It could be found that undoped anatase Titania exhibited the superior antibacterial efficiency compared with standard pure TiO_2 and other pure TiO_2 nanoparticles reported earlier.

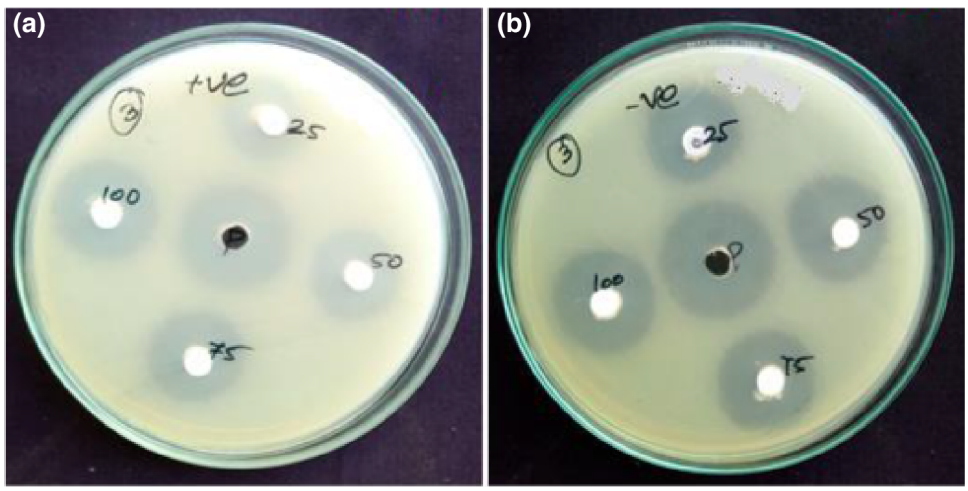

Fig. 7 showing antibacterial activity of Anatase TiO_2 from PIM -10 days calcined at 900 °C against **a** *S. aureus* and **b** *E. Coli*

Table 5 PIM- 10 days anatase TiO_2 as compared with zones of inhibition in case of control

Zone of inhibition level (in mm) (mean value of three measurements)					Control sample
Antibacterial activity	25 mg	50 mg	75 mg	100 mg	30 mg
G +ve	14.21 ± 0.68	17.33 ± 0.76	18.14 ± 1.04	20.23 ± 1.07	25.16 ± 0.76
G −ve	18.16 ± 0.66	20.33 ± 0.76	21.4 ± 0.65	23.3 ± 1.25	28.06 ± 0.70

Acknowledgements The authors thank lab Director Dr. P. Mohana sundram, PG Extension Centre, Periyar University, Dharmapuri-636107, Tamil Nadu, India for providing Lab facility to carry out this work and IITM for helping in characterizing the samples.

Compliance with Ethical Standards

Conflict of interest There are no conflicts to declare.

References

1. D. Jiang, J. Li, C. Xing, Z. Zhang, S. Meng, M. Chen, and A. C. S. Appl (2015). *Mater. Interfaces* **7**, 19234–19242.
2. J. Theerthagiri, A. P. Murthy, V. Elakkiya, S. Chandrasekaran, P. Nithyadharseni, Z. Khan, R. A. Senthil, R. Shanker, M. Raghavender, P. Kuppusami, J. Madhavan, and M. Ashokkumar (2018). *J. Ind. Eng. Chem.* **64**, 16–59.
3. M.R. Delsouz Khaki, M.S. Shafeeyan, A.A. Abdul Raman, W.M.A. Wan Daud, *J. Environ. Manag,* 2017, **198**, 78–94.
4. S. Y. Chae, C. S. Lee, H. Jung, O. S. Joo, B. K. Min, J. H. Kim, Y. J. Hwang, and A. C. S. Appl (2017). *Mater. Interfaces* **9**, 19780–19790.
5. R. A. Senthil, A. Priya, J. Theerthagiri, A. Selvi, P. Nithyadharseni, and J. Madhavan (2018). *Ionics* **24**, 3673–3684.
6. K. Wang, X. Wu, G. Zhang, J. Li, Y. Li, and A. C. S. Sustain (2018). *Chem. Eng* **6**, 6682–6692.
7. H. Wang, C. Wang, X. Cui, L. Qin, R. Ding, L. Wang, Z. Liu, Z. Zheng, and B. Lv (2018). *Appl. Catal. B Environ.* **221**, 169–178.
8. P. S. Kumar, S. A. S. Nizar, J. Solardaramurthy, P. Ragupathy, V. Thavasi, S. G. Mhaisalkar, and S. Ramakrishna (2011). *J. Mater. Chem* **21**, 9784–9790.
9. P.S. Kumar, V. Aravindan, J. Solardaramurthy, V. thavasi, S.G. Mhaisalkar, S. Ramakrishna, S. Madhavi, *RSC Adv*., 2012, **2**, 7983–7987.
10. S. Banerjee, D. D. Dionysiou, and S. C. Pillai (2015). *Appl. Catal. B Environ.* **176**, 396–428.
11. M. R. Mohammad, D. S. Ahmed, and M. K. A. Mohammed (2019). *J. Sol-Gel Sci. Technol.* **90**, 498–509.
12. D. S. Ahmed, M. K. A. Mohammed, and M. R. Mohamma (2020). *Chem. Pap.* **74**, 197–208.
13. M. K. A. Mohammed (2020). *Optik* **223**, 165607.
14. N. Sakai, R. Wang, A. Fujishima, and T. Watanabe (1998). *Langmuir* **14**, 5918–5920.
15. D. Christian, A. Miguel, P. Christopher, and S. Kley (2014). TiO_2 Anatase with a bandgap in the visible region. *Nano Lett.* **14**, 6533–6538.
16. M. Inagaki, R. Nonaka, B. Tryba, and A. W. Morawski (2006). *Chemosphere* **64**, 437–445.
17. N. Xu, Z. Shi, Y. Fan, J. Dong, and J. Shi (1999). *Ind. Eng. Chem. Res* **38**, 373–379.
18. B. Tryba (2007). *Appl. Catal. B Environ.* **71**, 163–168.
19. Y. B. Mao and S. S. Wong (2006). *J. Am. Chem. Soc.* **128**, 8217–8226.
20. W. F. Zhang, Y. L. He, M. S. Zhang, Z. Yin, and Q. Chen (2000). *J. Phys. D: Appl. Phys* **33**, 912–916.
21. J. C. Parker and R. W. Siegel (1990). *Appl. Phys. Letter* **57**, 943–945.
22. T. Ohsaka, S. Yamaoka, and O. Shimomura (1979). *Solid State Commun.* **30**, 345–347.
23. L. Kavan, M. Grtzel, S. E. Gilbert, C. Klemenz, and H. J. Scheel (1996). *J. Am. Chem. Soc.* **118**, 6716–6717.
24. V. Abbasi-Chianeh, A. Mohammadzadeh, and N. N. Ilkhechi (2019). *Journal of the Australian Ceramic Society* **55** (2), 355–362.
25. M. Alijani and N. N. Ilkhechi (2018). *Silicon.* **10** (6), 2569–2575.
26. G. Nagaraj, D. Brundha, C. Chandraleka, M. Arulpriya, V. Kowsalya, S. Sangavi, R. Jayalakshmi, S. Tamilarasu, and R. Murugan (2020). *SN Applied Sciences.* **2**, 734.
27. G. Nagaraj, A. Dhayal Raj, A. Albert Irudayaraj, R.L.Josephine. *Optik*,. 2019, **179**, 889–894.
28. V. Etacheri, M. K. Seery, S. J. Hinder, and S. C. Pillai (2011). *Adv. Func. Mater.* **21**, 3744–3752.
29. L.-L. Tan, W.-J. Org, S.-P. Chai, and R. S. C. Chem (2014). *Commun.* **50**, 6923–6926.
30. V. V. Jadhav, R. S. Dhabbe, S. R. Sabale, G. H. Nikam, and B. V. Tamhankar (2013). *Univ. J. Environ. Res. Tech.* **6**, 667–676.
31. L. Lv, Q. Chen, X. Liu, M. Wang, and X. Meng (2015). *J. Nanopart. Res.* **17**, 222–224.
32. K. Lv, J. Yu, L. Cui, S. Chen, and M. Li (2011). *J. Alloys and Comp.* **509**, 4557–4562.
33. J. T. Carneiro, T. J. Savenije, J. A. Moulijn, and G. Mul (2011). *J. Phys. Chem. C* **115**, 2211–2214.
34. H. D. Jang and S. K. Kim (2001). *J. Nanopart. Res.* **3**, 141–147.
35. T. Kawahara, T. Ozawa, M. Iwasaki, and H. Tada (2003). *J. Colloid Inter. Sci.* **267**, 377–378.
36. U. Stafford, K. A. Gray, P. V. Kamat, and A. Varma (1993). *Chem. Phys. Lett.* **205**, 55–61.
37. G. Riegel and J. R. Bolton (1995). *J. Phys. Chem.* **99**, 4215–4224.
38. G. Nagaraj, A. D. Raj, and A. A. Irudayaraj (2018). *J. Mater. Sci.: Mater. Electron.* **29**, 4373–4381.
39. P. Periyat, S. C. Pillai, D. E. McCormack, J. Colreavy, and S. J. Hinder (2008). *J. Phys. Chem. C* **112**, 7644–7652.
40. G. Nagaraj, R. A. Senthil, and K. Ravichandran (2019). *Materials Research Express* **6**, 095049.
41. T. Yoko, K. Kamiya, and K. Tanaka (1990). *J. Mater. Sci.* **25**, 3922–3929.
42. N. N. Ilkhechi, F. Dousi, B. K. Kaleji, and E. Salahi (2014). *Opt Quant Electron.* **47** (7), 1–13.
43. N. N. Ilkhechi, B. K. Kaleji, E. Salahi, and N. Hosseinabadi (2015). *Journal of sol-gel science and technology.* **74** (3), 765–773.
44. N.N. Ilkhechi, M. Alijani and B.K. Kaleji, B.K. *Optical and quantum electronics.* 2016, **48(2)**,148.
45. Y. Gao, Y. Masuda, Z. Peng, T. Yonezawa, and K. Koumoto (2003). *J. Mater. Chem.* **13**, 608–613.
46. S. A. Gao, A. P. Xian, L. H. CaO, and R. C. Xie (2008). *Sens. Actuators B Chem.* **134**, 718–726.

47. N. N. Ilkhechi, M. R. Akbarpour, R. Yavari, and Z. Azar (2017). *Journal of Materials Science: Materials in Electronics.* **28** (22), 16658–16664.
48. N. N. Ilkhechi and B. K. Kaleji (2016). *Optical and quantum electronics.* **48** (7), 347.
49. G. Nagaraj and R. A. Senthil (2020). Rajender Boddula, K. Ravichandran. *Current Analytical Chemistry* **16**, 1–6.
50. G. Nagaraj, D. Brundha, V. Kowsalya, C. Chandraleka, S. Sangavi, R. Jayalakshmi, M. Arulpriya, N. Sathya, M. Prasath and S. Tamilarasu. *Materials Today: Proceedings*.,2020.
51. K. S. Ong, Y. L. Cheow, and S. M. Lee (2017). *Journal of advanced research* **8** (4), 393–398.
52. M.S. Arif Sher Shah, K. Zhang, A.R. Park, K.S. Kim, N.-G. Park, J.H. Park, P.J. Yoo, *Nanoscale,* 2013, **5**, 5093–5101.
53. M. Gulluce, F. Sahin, M. Sokmen, H. Ozer, D. Daferera, and A. Sokmen (2007). *Food Chem.* **103**, 1449–1456.
54. D. Meng, X. Liu, Y. Xie, Y. Du, Y. Yang, and C. Xiao (2019). *Advances in Materials Science and Engineering.* **2019**, 1–9.
55. H.M. Yadav, S.V. Otari, V.B. Koli, S.S Mali, C.K. Hong, S.H. Pawar and S.D. *Journal of Photochemistry and Photobiology A: Chemistry*., 2014, **280**, 32–38